Supplemental Information for

Structures of VWF tubules before and after concatemerization reveal a mechanism of disulfide bond exchange

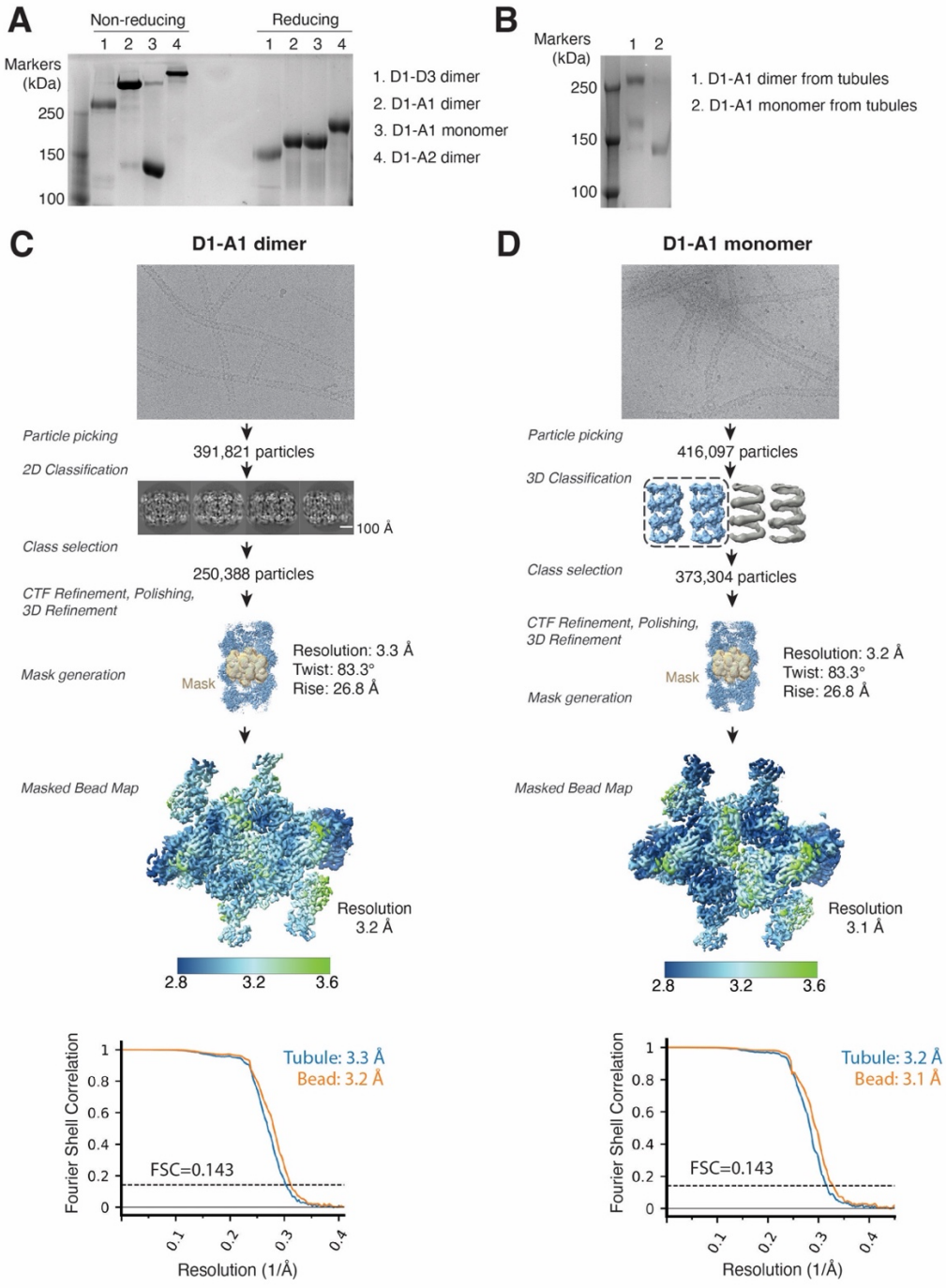

Figure S1. Cryo-EM processing. A. Purity of proteins used for tubule formation. All samples were run on a 5% SDS-PAGE gel. Samples on the right had a reducing agent in the loading buffer whereas samples

on the left were run in non-reducing conditions to preserve their disulfide-bond linkages. **B**. Non-reducing SDS-PAGE analysis of proteins after tubules were formed demonstrate that tubule formation was insufficient to cause monomers to dimerize. **C**. Flow diagram of the cryo-EM processing steps used to determine the structure of VWF tubules generated from the D1-A1 dimer. Below, Fourier shell correlation (FSC) curves for the tubule a central single bead, with the resolution at FSC=0.143 indicated. **D**. As C, but for VWF tubules generated from the D1-A1 monomer.

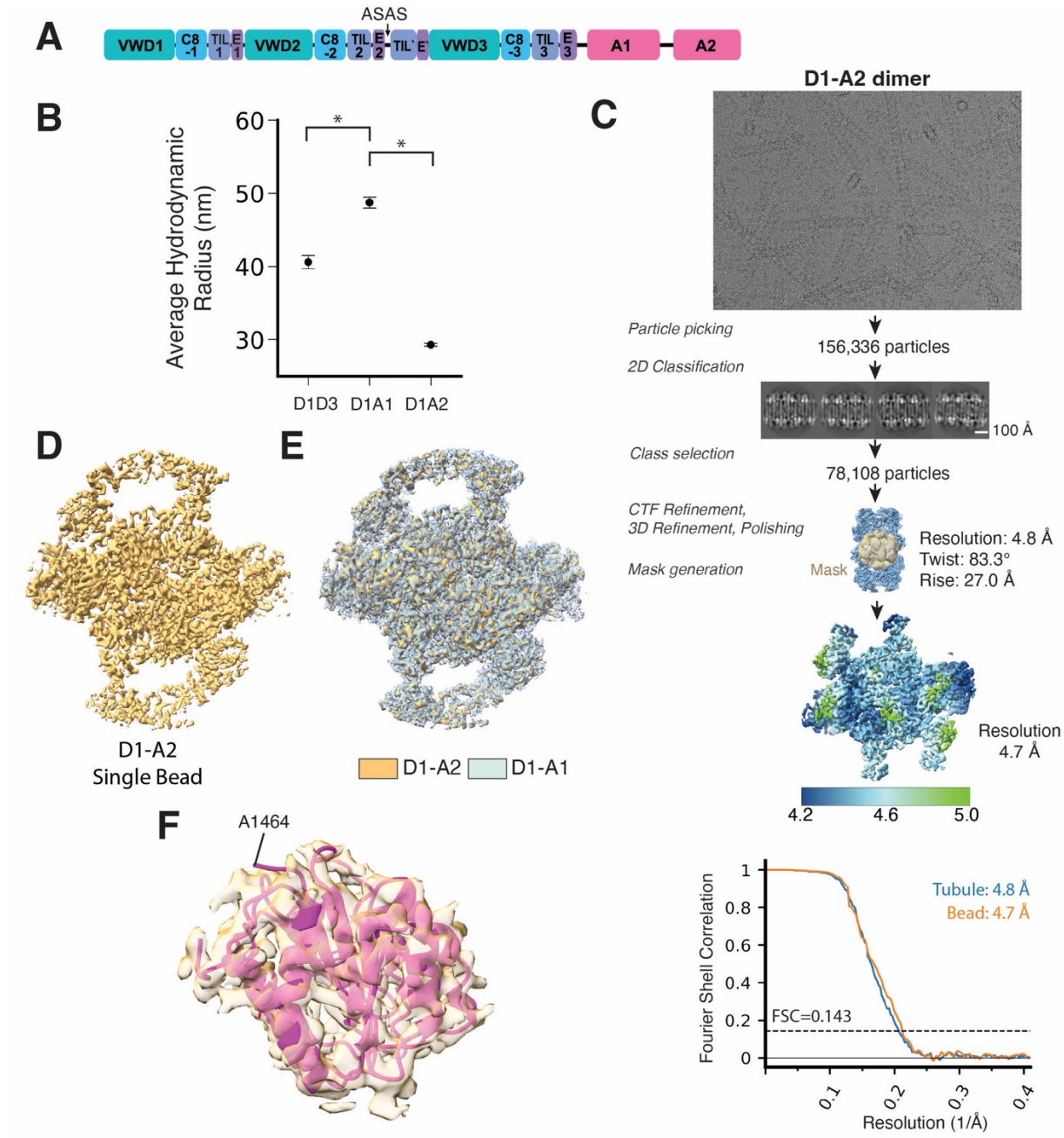

Figure S2. Cryo-EM processing of VWF tubules generated from a D1-A2 construct. A. Diagram of the D1-A2 construct. **B**. Hydrodynamic radius from dynamic light scattering (DLS) experiments of D1-D3, D1-A1, and D1-A2 after incubation at pH 5.2 for 24 hours. Error bars represent difference of the mean hydrodynamic radius across two replicates. Asterisks indicate two sample t-test p-value < 0.05. **C.** Flow diagram of the cryo-EM processing steps used to determine the structure of VWF tubules generated from purified D1-A2. Below, Fourier shell correlation (FSC) curves for the tubule and a single central bead, with the resolution at FSC=0.143 indicated. **D.** Density of a single D1-A2 bead. **E**. Overlay of the D1-A2 bead with transparent density from the D1-A1 dimer. No additional domains or domain

rearrangements are observed relative to the D1-A1 map. **F**. A1 model docked into the density of the A1 domain in D1-A2 tubules. No density is observed after residue A1464 for the A2 domain or linker to the A2 domain.

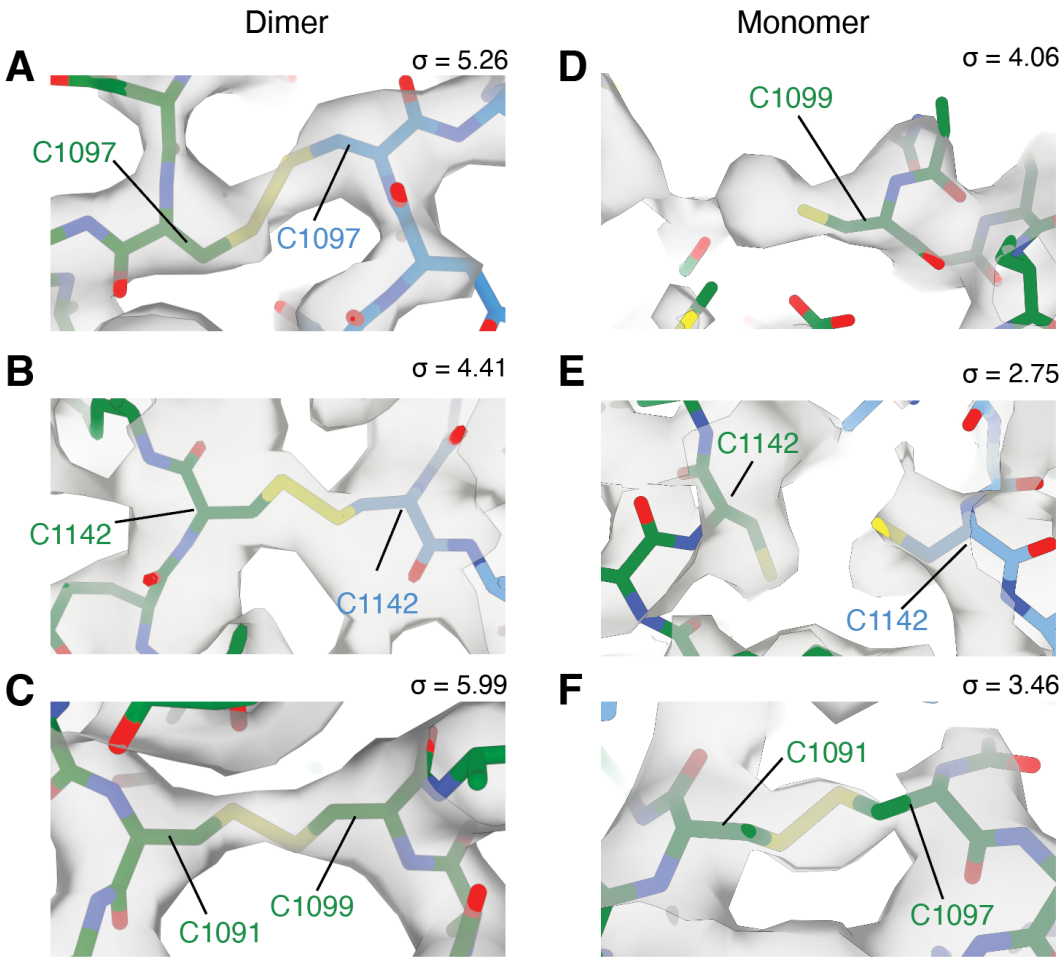

Figure S3. Cryo-EM map densities for mechanistically important cysteines and disulfide bonds. **A**. Density for the intermolecular C1097-C1097 disulfide bond in the D1-A1 dimer-derived tubule. **B**. Density for the intermolecular C1142-C1142 disulfide bond in the D1-A1 dimer-derived tubule. **C**. Density for the intramolecular C1091-C1099 disulfide bond in the D1-A1 dimer-derived tubule. **D**. Density for C1099 in the monomer-derived tubule. Unexplained density is seen adjacent to the sulfhydryl group. **E**. Density for C1142 in adjacent molecules in the monomer-derived tubule. **F**. Density for the intramolecular C1091-C1097 disulfide bond in the monomer-derived tubule. In all panels, the bonds are shown as sticks colored by element. Different molecules have carbons colored in green and blue, respectively. The cryo-EM maps were sharped with Phenix v1.19[22]. Contour level is indicated in the upper right of each panel.

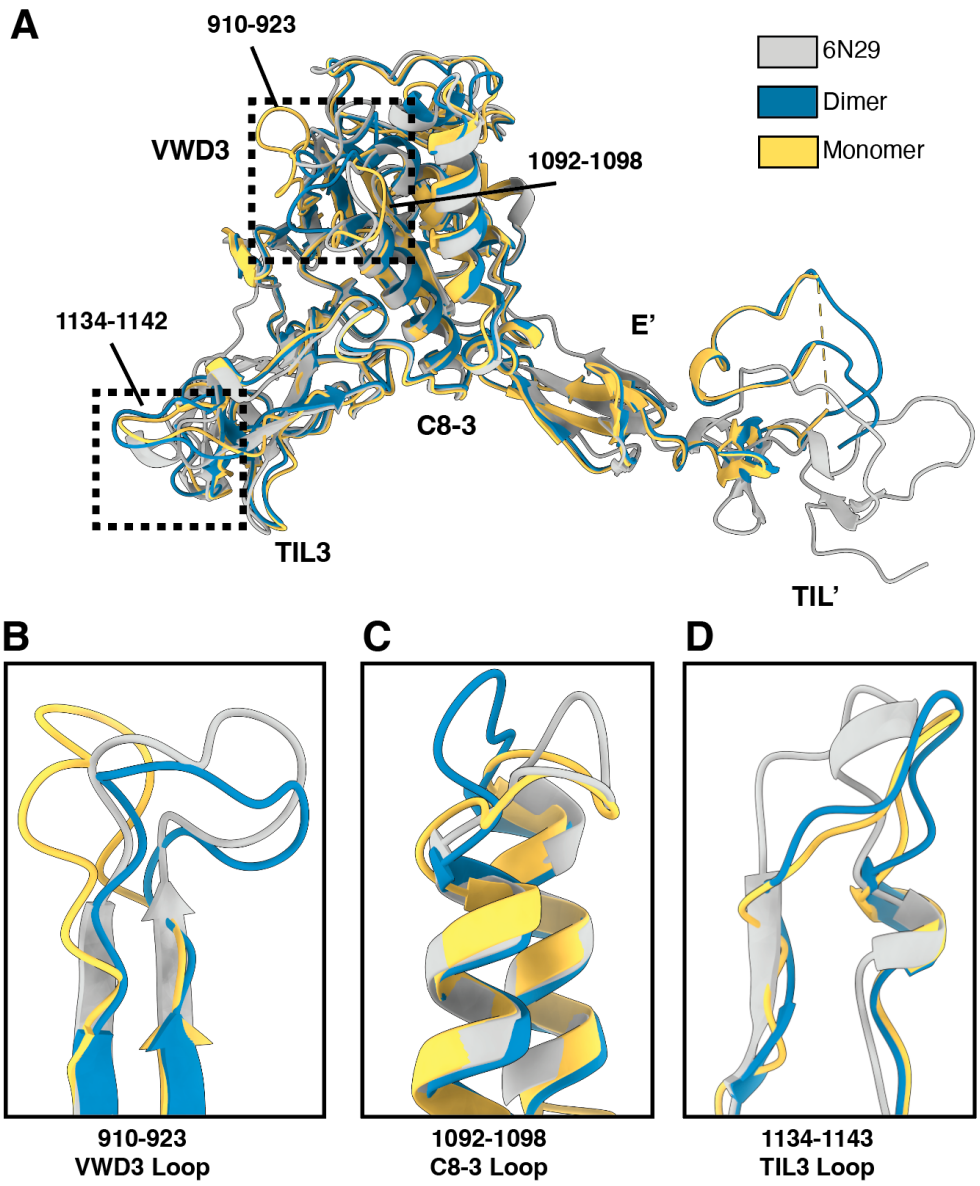

Figure S4. Superposition of atomic models of D′D3. **A.** Superposition of the D′D3 crystal structure (PDB: 6N29) [14] with atomic models determined from cryo-EM maps of VWF tubules assembled with either monomeric or dimeric D1-A1. The positions of interfacial loops highlighted in panels B-D are boxed. **B**. Superposition of the 910-923 loop. **C**. Superposition of the 1092-1098 loop. **D.** Superposition of the 1134-1143 loop. Superposition performed using the matchmake function of ChimeraX 1.3.

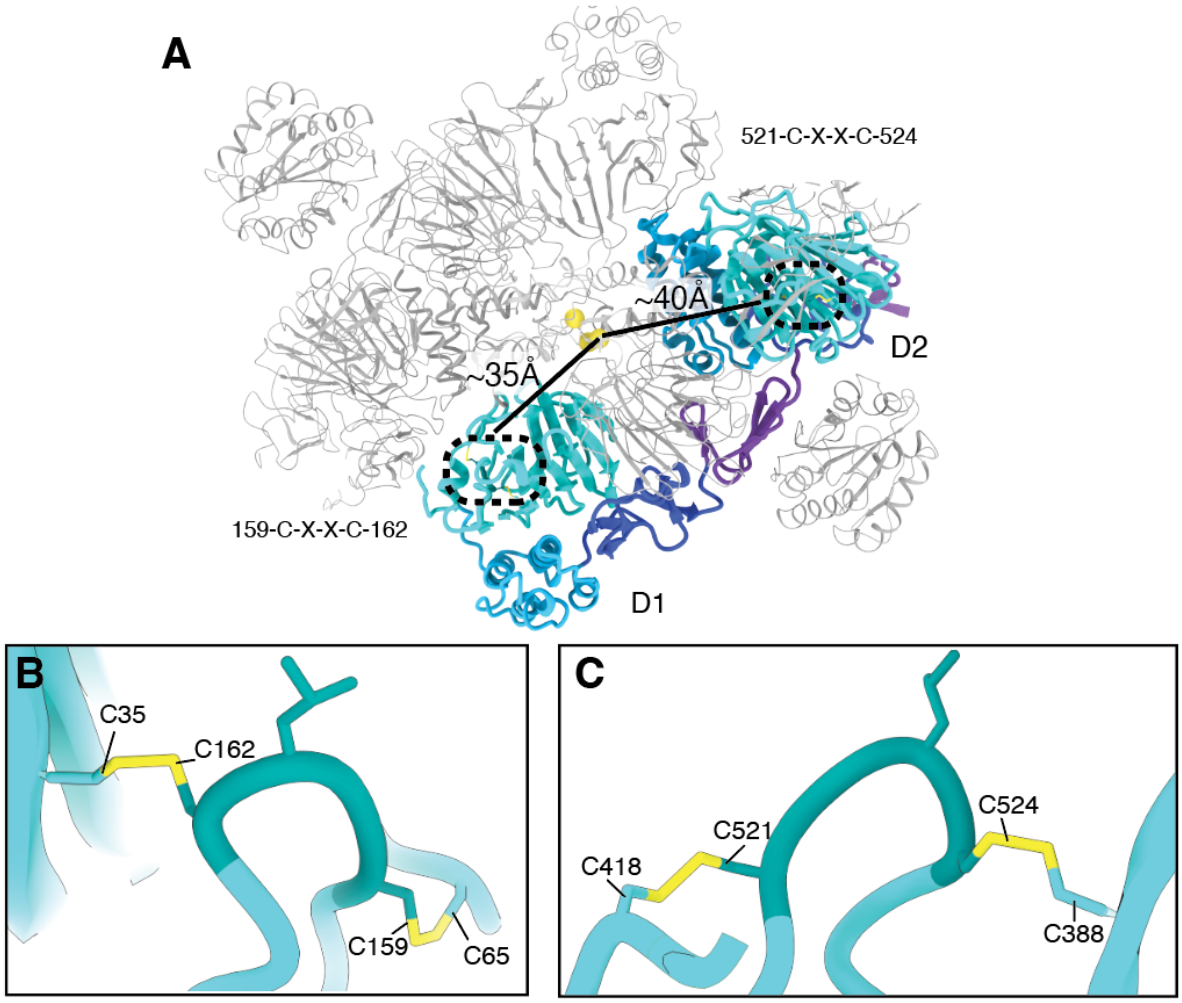

Figure S5. CXXC motifs in the prodomain are unlikely to catalyze disulfide exchange. **A**. Model of a single bead in grey with one D1 and D2 assembly colored by domain. Yellow spheres with 3 Å radius are placed at C1091, C1097, and C1099. Positions of CXXC motifs implicated in VWF intrinsic oxidoreductase activity[35] are denoted by dashed ellipses. The distance of each motif to C1099 is measured from the first cysteine. **B**. Atomic model depicting C159 and C162 of the D1 C159-XX-C162 motif in intramolecular disulfide bonds. **C**. Atomic model depicting C521 and C524 of the D2 C521-XX-C524 motif in intramolecular disulfide bonds.

Supplemental Movie Legends

Movie S1. Overview of the VWF tubule showing the organization of the VWF D1-A1 domains. The A1 domain is a component of the tubule wall that links helical repeats. Distinct molecules are denoted by no apostrophe, one apostrophe (’), or two apostrophes (’’).

Supplemental Tables

Table S1. Statistics for data collection, data processing, model refinement and validation.

	D1-A1 (monomer)	D1-A1 (dimer)	D1-A2 (dimer)
Data collection			
Microscope	Titan Krios	Titan Krios	Talos Artica
Detector	K3	K3	K3
Voltage (keV)	300	300	200
Nominal magnification	81,000	81,000	36,000
Electron exposure ($e^-/Å^2$)	55.52	55.46	53.06
Defocus range set during data acquisition (μm)	-0.6 to -2.0	-0.6 to -1.8	-1.2 to -2.2
Pixel size (Å)	1.06	1.06	1.1
Total movies acquired	12,996	6,121	1,065
Data Processing			
EMDB code	EMDB-27156	EMDB-27157	EMDB-27158
Particles	373,304	250,388	78,108
Helical Twist	83.3	83.3	83.3
Helical Rise	26.8	26.8	27.0
Map resolution (Å), Tubule Masked	3.2	3.3	4.8
Map resolution (Å), Single Bead Masked	3.1	3.2	4.7
Model composition			
PDB code	8D3C	8D3D	
Chains	16	16	
Atoms	162,720	163,856	
Residues	20,880	21,024	
Ligands	Ca^{2+}: 48, NAG: 80	$Ca^{2+:}$ 48, NAG: 80	
Refinement			
Resolution limit set in refinement (Å)	3.1	3.2	
Correlation coefficient (CCmask)	0.79	0.81	
C_{ref} (masked) (Å)	3.3	3.4	
Root-mean-square deviation (bond lengths) (Å)	0.004	0.007	
Root-mean-square deviation (bond angles) (Å)	1.125	1.042	
Validation			
MolProbity Score	1.05	1.17	
Clashscore	0.92	1.96	
Rotamer outliers (%)	0.35	0	
Ramachandran (favored) (%)	96.06	96.68	
Ramachandran (outliers) (%)	0	0	

Table S2. Analysis of VWF D1-A1 histidine residues. Structure-based analysis of all the histidine residues present in human VWF domains D1-A1 in the dimer-derived tubule structure. Conservation scores were determined using ConSurf [47]. pKa values were determined using pdb2pqr 3.4.1[48]. Abbreviations: WT = wild type.

Histidine	Location	Conser-vation Score	Structure-based pKa	Protonated upon pH drop (7.4 to 5.2)	Molecular environment	Effect of substitution on D1D3 dimerization[33]	Effect of substitution on VWF concatemerization [33]
95	VWD1	7	2.9	No	Near interface with C8-2 of neighbor. In an electronegative environment close to D75, D93 and D106.	Decreased	Slightly reduced
238	C8-1	7	5.7	Yes	Near interface with A1 domain.	WT levels	WT levels
288	C8-1	3	6.2	Yes	Faces solvent.		
316	TIL1	7	5.7	Yes	Near interface with VWD3 of neighbor.		
352	E1	9	3.8	No	Near interface with VWD3 of neighbor. Close to E1015 of neighbor.	WT levels	WT levels
395	VWD2	9	6.5	Yes	Potentially forms an intramolecular salt bridge with D611 of the C8-2 domain.	Prevented (H395A and H395R)	No concatemers (H395A or H395R/K)
421	VWD2	3	6.2	Yes	Faces solvent.		
452	VWD2	2	6.5	Yes	Near VWD2 of neighbor. May help neutralize charge of D467.		
460	VWD2	9	2.6	No	At interface with E2 of neighbor. Likely helps flanking R505 and K459 make salt bridges.	Prevented (H460L), Reduced (H460M/Q/A), Restored (H460R/K)	Impaired (H460A/L/M/Q) WT levels (H460K/R)
484	VWD2	4	5.4	Yes	7 Å from interface with VWD2 of neighbor.		
556	VWD2	5	5.5	Yes	In a histidine-rich region with H725/726 of neighboring molecule.		
566	C8-2	1	4.9	No	May interact with D437.		
596	C8-2	9	5.6	Yes	Near interface with C8-3 of neighbor. May interact with E593.	Decreased (H596A and H596R)	Reduced
725	E2	8	7.7	No	In a histidine-rich region.	WT levels	Impaired concatemerization
726	E2	3	6.3	Yes	In a histidine-rich region.		
737	E2	5	6.7	Yes	In an electronegative region at the interface with VWD1 of neighbor. Could neutralize electronegative charge.	Decreased (H737A and H737R)	Impaired concatemerization (H737A or H737R)
759	E2	5	-	-	Not resolved.		
817	TIL'	7	6.9	Yes	Potentially form intramolecular salt bridge with E835 of the E′ domain.		
831	TIL'	9	4.4	No	Potentially interacts with E543 of neighboring VWD2 domain. May form a water bridge with H1114.	WT levels	WT levels
861	TIL'	2	6.3	Yes	Faces solvent.		

874	VWD3	9	2.2	No	Likely coordinates a water molecule.	WT levels	WT levels
916	VWD3	3	5.2		On a flexible loop.		
952	VWD3	3	6.6	Yes	Potentially forms a salt bridge with E930 of same molecule.		
977	VWD3	3	5.8	Yes	In an electronegative environment surrounded by D975, D1096, and D1102.		
1047	C8-3	2	6.9	Yes	Potentially interacts with D1040,		
1109	C8-3	7	4.1	No	Forms intramolecular contacts.		
1114	C8-3	1	5.3	Yes	Potentially forms a water bridge with H831.		
1159	TIL3	9	6.6	Yes	May neutralize charge of acidic residues at the intramolecular interface with VWD3.	Impaired secretion	
1174	TIL3	8	5.0	No	Near glycosylation.	WT levels	WT levels
1176	TIL3	1	6.2	Yes	Near glycosylation.		
1221	E3	2	-	-	Not resolved	Reduced	WT levels
1226	E3	6	-	-	Not resolved	WT-levels	Reduced
1268	A1	6	6.0	Yes	Faces solvent		
1322	A1	8	3.8	No	At interface with E1. Forms a potential water bridge with H1326.		
1326	A1	7	3.1	No	At interface with E1. Forms a potential water bridge with H1322.		
1419	A1	3	5.8	Yes	Faces solvent		

Table S3. Analysis of single-residue substitutions associated with type 2A VW disease.
Abbreviations: HWM, high molecular weight; ER, endoplasmic reticulum; WPBs, Weibel-Palade bodies.

Mutation	Observations from structure	Evidence from literature
R202W	At interface between 3 molecules. Forms cation-π interactions with Y730 of neighboring E2 domain and electrostatic interactions with D168 and D434. A tryptophan substitution would disrupt electrostatic interactions but maintain stacking interactions.	Reduced HMW concatemers[38]
R273W	Likely forms an intramolecular salt bridge with D141 that would be lost by a substitution to tryptophan.	Patients lacked HMW concatemers in plasma. Mutation increased ER retention of recombinant VWF in COS-7 cells[49].
N528S	Involved in coordinating calcium. Loss may lead to a disruption of the calcium-binding site, which occurs at the VWD2-VWD3 interface.	Patients lack HMW concatemers. N528S-VWF variant showed only diffuse staining consistent with no WPBs. Increased ER retention[50].
G550R	An arginine substitution would affect intramolecular packing by generating a clash with F406.	Decreased levels of HMW concatemers[51]. Did not form WPBs potentially because of a secretion defect[52].
S979N	May disrupt intramolecular packing.	S979N might be associated with VW disease type 2E[53].
G1180R	Faces solvent. Substitution may decrease local structural flexibility.	Reduced HMW concatemers but not replicated with recombinant VWF protein secreted into media[54].
L1276P	Could prevent proper folding of the hydrophobic core of the A1 domain.	Patients lacked HMW concatemers in plasma[40].
V1279F	Could prevent proper folding of the hydrophobic core of the A1 domain.	Absence of HMW concatemers[55].
L1307P	Could prevent proper folding of the hydrophobic core of the A1 domain.	Marginal decrease of the largest VWF concatemers. Reduced production and increased ER retention. Mainly short/round WPBs[39].
V1316M	Could prevent proper folding of the hydrophobic core of the A1 domain.	Reduced HMW concatemers[56]. Also associated with severe thrombocytopathy[57].
R1374H	May affect folding of the A1 domain.	Reduced HMW concatamers.[58]

Supplemental References

48. Jurrus E, Engel D, Star K, et al. Improvements to the APBS biomolecular solvation software suite. *Protein Sci.* 2018;27(1):112-128. https://doi.org/10.1002/pro.3280

49. Allen S, Abuzenadah AM, Hinks J, et al. A novel von Willebrand disease-causing mutation (Arg273Trp) in the von Willebrand factor propeptide that results in defective multimerization and secretion. *Blood.* 2000;96(2):560-568. https://doi.org/10.1182/blood.V96.2.560

50. Haberichter SL, Budde U, Obser T, Schneppenheim S, Wermes C, Schneppenheim R. The mutation N528S in the von Willebrand factor (VWF) propeptide causes defective multimerization and storage of VWF. *Blood.* 2010;115(22):4580-4587. https://doi.org/10.1182/blood-2009-09-244327

51. Schneppenheim R, Thomas KB, Krey S, et al. Identification of a candidate missense mutation in a family with von Willebrand disease type IIC. *Hum Genet.* 1995;95(6):681-686. https://doi.org/10.1007/BF00209487

52. Brehm MA, Obser T, Budde U, Blood SS. Subcellular localization of von Willebrand factor mutants correlates with particular VWF multimer patterns. *Blood.* 2012;120(21):98. https://doi.org/10.1182/blood.V120.21.98.98

53. Michiels JJ, Smejkal P, Mayger K, et al. Combined use of rapid von Willebrand factor (VWF) activity, VWF-propetide and classical VWF assays for improved diagnosis of von Willebrand disease type 1, 2N and 2E due to mutations in the D1, D2, D', D3 and D4 domains of the VWF gene. *Thromb Haemost Res*. 2019;3(2):1027.

54. James PD, O'Brien LA, Hegadorn CA, et al. A novel type 2A von Willebrand factor mutation located at the last nucleotide of exon 26 (3538G>A) causes skipping of 2 nonadjacent exons. *Blood.* 2004;104(9):2739-2745. https://doi.org/10.1182/blood-2003-12-4286

55. Corrales I, Ramírez L, Altisent C, Parra R, Vidal F. Rapid molecular diagnosis of von Willebrand disease by direct sequencing. Detection of 12 novel putative mutations in VWF gene. *Thromb Haemost.* 2009;101(3):570-576. https://doi.org/10.1160/TH08-08-0500

56. Jackson SC, Sinclair GD, Cloutier S, Duan Z, Rand ML, Poon MC. The Montreal platelet syndrome kindred has type 2B von Willebrand disease with the VWF V1316M mutation. *Blood.* 2009;113(14):3348-3351. https://doi.org/10.1182/blood-2008-06-165233

57. Casari C, Berrou E, Lebret M, et al. von Willebrand factor mutation promotes thrombocytopathy by inhibiting integrin αIIbβ3. *J Clin Invest.* 2013;123(12):5071-5081. https://doi.org/10.1172/JCI69458

58. Castaman G, Eikenboom JC, Rodeghiero F, Briët E, Reitsma PH. A novel candidate mutation (Arg611-->His) in type I 'platelet discordant' von Willebrand's disease with desmopressin-induced thrombocytopenia. *Br J Haematol.* 1995;89(3):656-658. https://doi.org/10.1111/j.1365-2141.1995.tb08383.x